Sparse Gradient Image Reconstruction from Incomplete Fourier Measurements and Prior Edge Information

K. Chowdhary, J. Hesthaven, E. Walsh

In many imaging applications, such as functional Magnetic Resonance Imaging (fMRI), full, uniformly-sampled Cartesian Fourier (frequency space) measurements are acquired to reconstruct an image. In order to reduce scan time and increase temporal resolution for fMRI studies, one would like to accurately reconstruct these images from the smallest possible set of Fourier measurements. The emergence of Compressed Sensing (CS) has given rise to techniques that can provide exact and stable recovery of sparse images from a relatively small set of Fourier measurements. In particular, if the images are sparse with respect to their gradient, e.g., piece-wise constant, total-variation minimization techniques can be used to recover those images from a highly incomplete set of Fourier measurements. In this paper, we propose a new algorithm to further reduce the number of Fourier measurements required for exact or stable recovery by utilizing prior edge information from a high resolution reference image. This reference image, or more precisely, the fully sampled Fourier measurements of this reference image, is obtained prior to an fMRI study in order to provide approximate edge information for the region of interest. By combining this edge information with CS techniques for sparse gradient images, numerical experiments show that we can further reduce the number of Fourier measurements required for exact or stable recovery by a factor of $1.6 - 3$, compared with CS techniques alone, without edge information.

1   Introduction

Magnetic Resonance Imaging (MRI) is a widely used medical imaging technique to visualize detailed soft tissue structures of the body, e.g., brain, muscles, heart, etc. Due to its ability to employ contrast weightings based on physiological function, e.g. perfusion, MRI has led to the development of functional Magnetic Resonance Imaging (fMRI) requiring the acquisition of time series information, i.e., a set of images at different time points [16]. An important consideration in fMRI is the total scan time required to obtain an accurate representation of the the region of interest (which determines the temporal resolution of the time series). Temporal resolution must be adequate for rendering the time varying property (contrast change due to changes in local blood flow and oxygenation). For example, on a typical clinical scanner, the achievable temporal resolution using conventional echo-planar acquisitions with whole-brain coverage is on the order of 2-2.5 seconds. Thus, a reduction in total scan time and improved temporal resolution for fMRI is highly desirable, especially for functional connectivity studies. Because MRI and fMRI techniques acquire a set of Fourier or frequency space measurements for image reconstruction [13, 14], an obvious solution to this problem is to reduce the amount of frequency space information obtained for each image and time point.

One method of reducing the amount of Fourier or frequency space measurements is

based on the theory of Compressed Sensing (CS). CS indicates that it is possible to reconstruct an image accurately, and sometimes even exactly, from random, incomplete Fourier measurements [3, 5]. The set of Fourier measurements are incomplete in the sense that one cannot simply perform a discrete Fourier transform (DFT) matrix inversion to recover the image. The Nyquist-Shannon sampling theorem tells us that in order to reconstruct the image exactly, we need to acquire the same number of Fourier measurements as the resolution of the image. However, CS suggests that accurate recovery can be achieved by sampling far fewer Fourier measurements than specified by Nyquist-Shannon.

Many types of images exhibit sparsity in some domain, e.g. Fourier, gradient, wavelet, etc. In this paper, we will focus on images that exhibit sparsity with respect to their gradients. For example, consider the widely used Shepp-Logan phantom image [20] in Figure 0.

Figure   1: (Left) 256×256 Sparse Gradient Shepp-Logan phantom image. (Right) Nonzero horizontal and vertical discrete gradient information.

Using CS, it is possible to recover a sparse gradient image from random Fourier measurements via a convex ℓ_1-minimization problem. More precisely, a K-sparse gradient image $X \in C^{N \times N}$, i.e., X has only K nonzero gradients, can be recovered exactly from only $m \geq O(K \log^4 N^2)$ discrete Fourier measurements, chosen uniformly at random, via a convex ℓ_1-minimization problem [5, 19, 18, 3]. In practice this bound is much too conservative and it is conjectured that a theoretical lower bound of $O(K \log N)$ is possible [17]. In comparison, the Nyquist-Shannon sampling theorem requires that all N^2 discrete Fourier measurements are required for exact reconstruction.

In this paper, we propose a new method to further reduce the amount of Fourier measurements, while still obtaining exact or stable reconstruction, by utilizing additional, prior edge information from a high-resolution reference image. In this context, the edge information of a reference image $Y \in C^{N \times N}$ refers to both the indices for which the gradient is nonzero and the corresponding gradient magnitudes.[1] The reference image itself is not acquired directly, but rather the full sampled two-dimensional Fourier measurements $\hat{Y} \in C^{N \times N}$ are obtained. The Fourier transform information of this reference image is typically acquired prior to an fMRI time series study and is used for grey/white matter segmentation. Under the assumption that both the reference image and sparse-gradient time series images share similar

---

[1]For an image $Y \in C^{N \times N}$ the gradient refers to the horizontal and vertical first-order finite differences.

edge information, our proposed algorithm seeks to reduce the number of Fourier measurement by combining CS techniques for sparse-gradient images with edge information from the Fourier measurements of the reference image. Figure 1 shows an example of a reference image (left) and a sparse gradient image at a single time point (right). These two images share almost identical edge information except for different magnitudes in their gradients. Figure 2 shows a cross-section of the two images to illustrate the difference between their gradients. This represents the case where the reference image is acquired at the same resolution as the time series images. The case where the reference image is acquired at higher spatial resolution than the time series is discussed subsequently.

Figure 2: (Left) Reference image from which we have fully sampled Fourier measurements taken prior to the fMRI study. (Right) Image at a single time point, which we are trying to reconstruct from incomplete Fourier measurements.
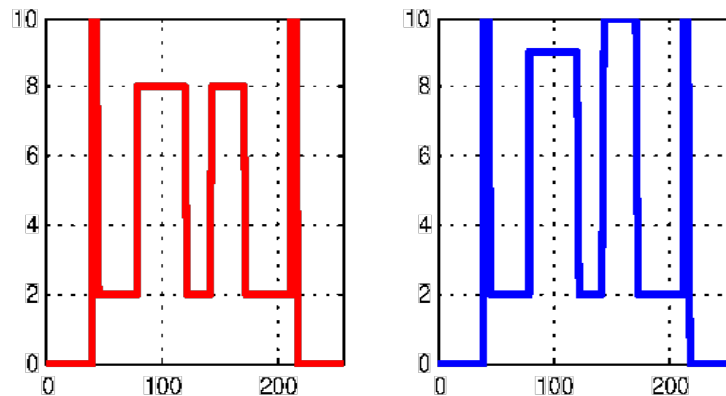

Figure 3: Comparison of center cross section of the two images in Figure 1. The red cross section (left) shows the reference image and the blue cross-section shows the image at a single time point.

In order to extract edge information from the Fourier measurements of the reference image, we will utilize the theory developed in a series of papers by Gelb and Tadmor on the detection of edges from Fourier coefficients [7, 6, 8]. This will allow us to determine approximate edge information about the sparse gradient time series. Then, by properly combing this approximate edge information with the Fourier measurements of the time series images via our proposed algorithm, we will show that the number of Fourier measurements

required for accurate, or even exact, reconstruction is significantly lower than for the total variation technique alone.

This paper is organized as follows. Section 2 introduces the idea of gradient sparsity and the basic problem setup. Section 3 reviews the theory of CS applied to sparse-gradient images. Section 4 summarizes the basic concepts of edge detection from Fourier coefficient data, and explains how one can extract the relevant edge information from the reference image. Section 5 introduces the main algorithm which combines CS techniques for sparse-gradient images (Section 3) with edge information from the reference image (Section 4). Finally, Section 6 presents three sets of numerical experiments for the reconstruction of a time series from its Fourier measurements and prior edge information using our proposed algorithm.

2   Setup and Problem Formulation

Consider an image $X \in C^{N \times N}$ and a reference image $Y \in C^{N \times N}$, for which we have full discrete Fourier transform information, $\hat{Y} \in C^{N \times N}$. Let us refer to the individual pixels of the image X by $X_{i,j}$ and let $n = N^2$. Define the horizontal and vertical differencing matrices (same as in [2])

$$
\begin{aligned}
(D_h X)_{i,j} &:= \begin{cases} X_{i+1,j} - X_{i,j} & i < N \\ 0 & i = N \end{cases} \\
(D_v X)_{i,j} &:= \begin{cases} X_{i,j+1} - X_{i,j} & j < N \\ 0 & j = N \end{cases}
\end{aligned}
$$

and the discrete gradient operator

$$
(DX)_{i,j} = \begin{pmatrix} (D_h X)_{i,j} \\ (D_v X)_{i,j} \end{pmatrix}
$$

where $DX \in C^{N \times N \times 2}$. The discrete isotropic and anisotropic total variation operator can be defined as

$$
\begin{aligned}
\left(TV_{iso}(X)\right)_{i,j} &= \sqrt{|(D_h X)_{i,j}|^2 + |(D_v X)_{i,j}|^2}, \\
\left(TV_{aniso}(X)\right)_{i,j} &= |(D_h X)_{i,j}| + |(D_v X)_{i,j}|
\end{aligned}
$$

where $TV_{iso}(X), TV_{aniso}(X) \in C^{N \times N}$, respectively. The ℓ_p norm for $0 < p < \infty$ is defined as

$$
\|X\|_p = \left(\sum_{i=1}^{N} \sum_{j=1}^{N} |X_{i,j}|^p \right)^{1/p} \tag{1}
$$

For $p = 0$ we have the quasi-norm

$$
\|X\|_0 = \left\{ \#(i,j) : X_{i,j} \neq 0 \right\}
$$

which counts the number of nonzero elements in X. Let us define the isotropic and anisotropic total-variation quasi-norm as

$$
\begin{aligned}
\|X\|_{TV_{iso}} &= \|TV_{iso}(X)\|_1, \\
\|X\|_{TV_{aniso}} &= \|TV_{aniso}(X)\|_1.
\end{aligned}
$$

X is K sparse if $\|X\|_0 = K$ and X is K-sparse in total-variation or gradient if

$PTV_{iso}(X)P_0 = K$ or $PTV_{aniso}(X)P_0 = K$ in the isotropic or anistropic discretization, respectively. From here on, we will only consider the anistropic discretization, but all theoretical results apply analogously to the isotropic form as well.

The goal is to recover an image X, which is K-sparse in gradient, from $m = n$ Fourier measurements of X and full Fourier information in $\hat{Y}$, via edge information, .[2] Define the set Ω of M two-dimensional frequencies $(\omega_{1,k}, \omega_{2,k})$ for $1 \le k \le m$ chosen according to some sampling pattern from the set $\{1, \ldots, n\}$, e.g., uniform random sampling. Let F denote the normalized one-dimensional $N \times N$ DFT matrix and F^{-1} its inverse, where

$$F_{i,j} \quad = \quad \frac{1}{\sqrt{N}} e^{2\pi(i-1)(j-1)/N}, \quad i, j = 1, \ldots, N.$$

Also, let F denote the two-dimensional DFT and F^{-1} its inverse. One can write the operator F in terms of F as

$$\mathsf{F}X \quad = \quad FXF.$$

Define the restricted two-dimensional Fourier operator $\mathsf{F}_\Omega : C^{N \times N} \to C^m$, where

$$\left(\mathsf{F}_\Omega X\right)_k \quad = \quad \left(\mathsf{F}X\right)_{(\omega_{1,k}, \omega_{2,k})}.$$

For a reference image Y, the edge or jump locations refer to the pixels or indices for which $TV_{aniso}(Y)$ is nonzero, and the edge or jump magnitudes refer to the corresponding value of $TV_{aniso}(Y)$ at those jump locations. The edge information of an image Y refers to the collection of edge or jump locations and the corresponding edge or jump magnitudes. Because Fourier transform information about Y is given (instead of Y itself), we will utilize the theory of edge detection from Fourier measurements in order to extract the relevant edge information (see Section 4).

The problem can now be stated as follows: Consider a set Ω of $m = n$ Fourier measurements, $\mathsf{F}_\Omega X$, and edge information from a reference image Y, taken from the two dimensional Fourier information $\hat{Y} = \mathsf{F}Y$. Let us assume that the reference image exhibits similar edge information as the sparse gradient image X. Can we recover X from far fewer Fourier measurements than CS techniques alone would allow by using prior edge information in Y? In short, can we reduce m when we have information about the edges?

3   Sparse Reconstruction from Fourier measurements

In this section we review CS theory for the reconstruction of total variation or gradient sparse images from incomplete Fourier measurements. Consider an image X with Fourier measurements $\mathsf{F}_\Omega X$. One can recover the image X via ℓ_1 total-variation minimization

$$X^* = \arg\min_Z PTV_{aniso}(Z)P_1 \quad \text{subject to} \quad \mathsf{F}_\Omega Y = \mathsf{F}_\Omega X. \tag{2}$$

The following proposition tells when the ℓ_1 total-variation minimization recovers X.

---

[2]We postpone the discussion of edge detection from Fourier data $\hat{Y}$ until Section 4, where the proper foundations are laid.

Proposition 1 *Let X be real-valued and K sparse in the gradient or total-variation domain, using the isotropic or anistropic discretization. If $m \geq CK \log^4(N)$ and the measurements are chosen uniformly at random, then the solution to the ℓ_1 minimization problem of (2)(is unique and equal to X with probability at least $1 - N^{-\gamma \log^3(N)}$, where $C, \gamma > 1$ are universal constants that do not depend on m or N.*

The proof for the above proposition is based on the work in [5] and an extension in [3]. It is conjectured that the lower bound may in fact be $O(K \log(N))$ (see [3] and [17]). If the measurements contain noise,

$$y \;=\; \mathsf{F}_\Omega X + \eta$$

where η is the measurement noise with $\mathsf{P}\eta\mathsf{P}_2 = \varepsilon$ and $y \in C^m$ the noisy measurements, one can solve

$$X_\eta^* = \arg \min_Z \mathsf{P}TV_{aniso}(Z)\mathsf{P}_1 \quad \text{s.t.} \quad \mathsf{P}\mathsf{F}_\Omega X - b\mathsf{P}_2 \leq \varepsilon. \tag{3}$$

Then, the solution to (3) is guaranteed to satisfy $\mathsf{P}X - X_\eta^*\mathsf{P}_2 \leq C_1\eta$ where C depends on the number of measurements (see [5], Theorem 3.5). Thus, we can achieve stable recovery in the presence of noisy measurements.

One can solve (2) or (3) via an unconstrained optimization approach of the form

$$X_\lambda^* = \arg \min_Z \lambda \mathsf{P}TV_{aniso}(Z)\mathsf{P}_1 + \mathsf{P}\mathsf{F}_\Omega X - b\mathsf{P}_2^2, \tag{4}$$

where $\lambda \geq 0$ is a penalization parameter. This positive scalar can be chosen small enough so that $\mathsf{P}\mathsf{F}_\Omega X - b\mathsf{P} \leq \varepsilon$ in the noisy case. In the noiseless case, it can be shown that $\lim_{\lambda \to 0} X_\lambda^* = X^*$ (see [18]).

4 Edge Detection in Fourier Data

In a series of papers by Gelb and Tadmor ([7], [6], and [8]), the authors provide the mathematical framework and computational methods for detecting edges from Fourier coefficient of piecewise smooth, periodic functions. The purpose of this section is to introduce these ideas and techniques and apply them to the reference image in order to extract the relevant edge information. We begin with a short review of the basic concepts and results from this series of work and end by introducing the edge detection operator.

Consider a 2π periodic and piecewise smooth function $f(x)$ on the interval $[0, 2\pi)$ with a single jump at $x = \xi$. Assume that a one sided p^{th} derivative of $f(x)$ exists at $x = \xi$ for $m \geq 1$ (obviously piecewise constant functions will satisfy this assumption).[3] Define the jump of the function $f(x)$ as

$$[f](x) \;:= \; f(x^+) - f(x^-)$$

---

[3]The results and analysis are the same for functions with finitely many jumps, but for simplicity we only consider one such jump.

where $f(x^+)$ and $f(x^-)$ are the right and left side limits of $f(x)$ at x, respectively. Suppose we are given the Fourier coefficients of $f(x)$

$$\hat{f}_k = \frac{1}{2\pi}\int_0^{2\pi} f(x)e^{-ikx}dx$$

for $k = -N,\ldots,N$. A classical method of detecting edges from these Fourier coefficients is based on evaluating the conjugate Fourier partial sum of the form

$$-\frac{\pi}{\log(N)}\widetilde{S}_N[f](x) = -\frac{i\pi}{\log(N)}\sum_{k=-N}^{N} sgn(k)\hat{f}_k e^{ikx}, \tag{5}$$

where sgn is the signum function. It can be shown (see [1], or [7], Theorem 2.1) that $-\frac{\pi}{\log(N)}\widetilde{S}_N[f](x)$ converges to $[f](x)$ at a rate of $O(1/\log(N))$. To speed up the convergence, the authors introduced a generalized conjugate Fourier sum

$$\widetilde{S}_N^\sigma[f](x) = i\sum_{k=-N}^{N} sgn(k)\sigma\left(\frac{|k|}{N}\right)\hat{f}_k e^{ikx} \tag{6}$$

where $\sigma(\eta) = \sigma(\frac{|k|}{N}), \eta \in (0,1]$ is called a concentration factor. Under an admissible concentration function (see [7], Definition 2.1), the generalized conjugate partial sum in (6) will converge much faster than (5). In particular, if one takes a first-degree polynomial concentration factor $\sigma(x) = -\pi x$ or

$$\sigma_{k,N} \equiv -\frac{\pi k}{N} \tag{7}$$

then, according to Theorem 3.1 in [7],

$$\widetilde{S}_N^\sigma[f](x) \stackrel{N\to\infty}{\to} [f](x)$$

at a rate of $O(\frac{\log(N)}{N})$. One can think of $\sigma_{k,N}$ as a reverse filter in the sense that it amplifies the higher Fourier modes. There are numerous other concentration factors introduced in [7], Section 3.4, but in this paper we will only use the one shown in (7).

In the discrete case, even after applying the concentration factor, spurious oscillations may appear, as seen in Figure 3.
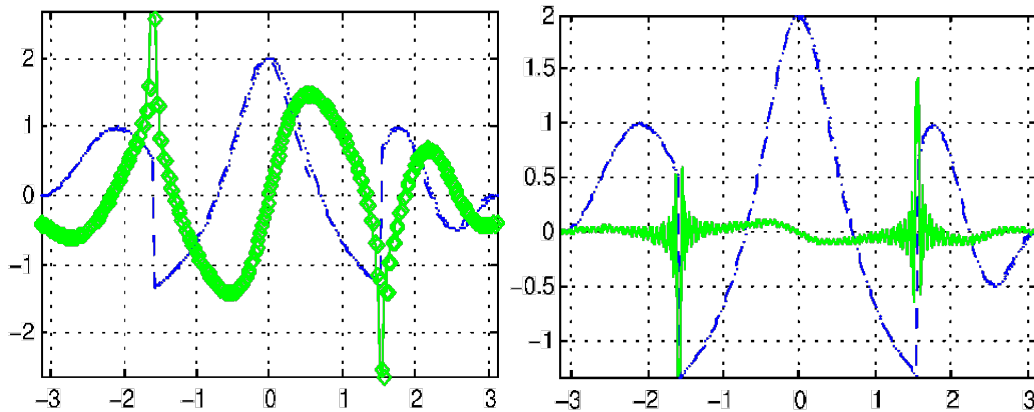

Figure   4: (Left) Conjugate partial sum, shown in green, of $f(x)$, shown as the blue

dotted line, with two jumps. (Right) Generalized conjugate partial sum with a first-degree polynomial concentration factor, shown in green, of $f(x)$, shown as the dotted blue line.

In this case, filtering can be used to dampen the oscillations. A number of different filters are discussed in [10], Chapter 9. In this paper, we will use an exponential filter of the form

$$\sigma^{\text{filt}}(\eta) \;=\; \begin{cases} 1 & |\eta| \le \eta_c \\ \exp\!\left(-\alpha\left(\dfrac{\eta - \eta_c}{1 - \eta_c}\right)^{p}\right) & \eta > \eta_c \end{cases},$$

where $\eta \in (0,1]$, α is a measure of the how strong the higher modes should be filtered, and p is the order of the filter. With the addition of the exponential filter, our new generalized conjugate Fourier sum takes on the form

$$\widetilde{S}_N^{\sigma}[f](x) = i \sum_{k=-N}^{N} sgn(k)\sigma\!\left(\frac{|k|}{N}\right)\sigma^{\text{filt}}\!\left(\frac{|k|}{N}\right)\hat{f}_k e^{ikx}. \tag{8}$$

Figure 4 shows the generalized conjugate partial sum after the exponential filter has been added. The oscillations are virtually eliminated.
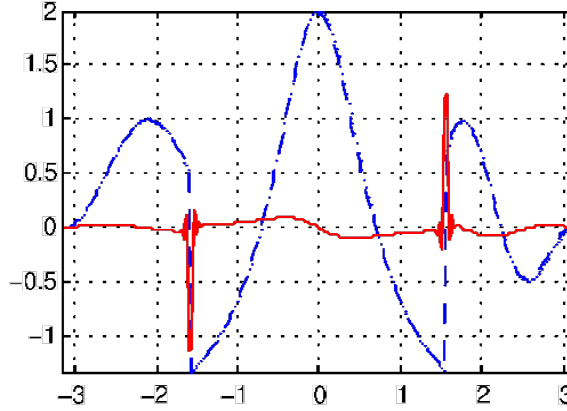

Figure 5: Generalized conjugate partial sum with exponential filter.

For a signal $x \in C^N$ we can define an edge matrix $E \in C^{N \times N}$ to be the discrete analog to $\widetilde{S}_N^{\sigma}$. Then, E has the form

$$E \;:=\; F^{-1}\Sigma F \tag{9}$$

where

$$\Sigma := diag\!\left(\frac{1}{\log(N/2)}isgn(\tilde{k})\sigma\!\left(\frac{2|\tilde{k}|}{N}\right)\sigma^{\text{filt}}\!\left(\frac{2|\tilde{k}|}{N}\right)\right), \quad \tilde{k} := \left(0,\ldots,\frac{N}{2},-\frac{N}{2}+1,\ldots,-1\right),$$

is a diagonal $N \times N$ complex valued matrix, and recall that $F \in C^{N \times N}$ is the one-dimensional discrete Fourier matrix.

A two-dimensional image X will have edge information along the horizontal and vertical directions. Thus, E must be applied along the rows and columns of a discrete image X. Define the two dimensional edge detection operator as

$$\mathsf{E}X \quad := \quad \begin{pmatrix} EX \\ XE^T \end{pmatrix} \tag{10}$$

where $EX \in C^{N \times N}, XE^T \in C^{N \times N},$ and $\mathsf{E}X \in C^{2N \times N}$. Furthermore, in order to apply this operator E to the two-dimensional Fourier transform information, $\hat{Y}$, E must be further modified.[4] The operator that applies to $\hat{Y}$ will be of the form

$$\hat{\mathsf{E}}\hat{Y} \quad := \quad \begin{pmatrix} \hat{E}\hat{Y}F^{-1} \\ F^{-1}\hat{Y}\hat{E}^T \end{pmatrix} \tag{11}$$

where $\hat{E} := F^{-1}\Sigma$, $\hat{E}\hat{Y}F^{-1} \in C^{N \times N}, F^{-1}\hat{Y}\hat{E}^T \in C^{N \times N},$ and $\hat{\mathsf{E}}\hat{Y} \in C^{2N \times N}$.

For our method, one does not need all the the edge information contained in $\hat{\mathsf{E}}\hat{Y}$ - only the information at the locations of the jumps. In order to determine the relevant data, let us introduce a threshold parameter $\tau > 0$ and search for the indices in $\hat{\mathsf{E}}\hat{Y}$ for which the pixel values surpass this threshold. The threshold parameter can be empirically determined so that it is small enough to capture the most significant jumps. These steps are summarized below.

      1.   Empirically estimate $\tau > 0$ so that τ is small enough to capture the relevant jumps.

      2.   After computing $\hat{\mathsf{E}}\hat{Y}$, we determine the indices for which the pixel values are larger than the threshold, $\tau > 0$, in absolute magnitude. More precisely, let

$$\Omega_\tau' \quad := \quad \left\{ (i,j) \quad : \quad \begin{matrix} |(\hat{\mathsf{E}}\hat{Y})_{i,j}| \geq \tau, \\ 1 \leq i \leq 2N, \quad 1 \leq j \leq N \end{matrix} \right\}$$

where $m_\tau := |\Omega_\tau'|$ is the cardinality of the set Ω_τ'. For convenience, we define Ω_τ to be set of m_τ pairs $(i_k, j_k) \in \Omega_\tau'$ for $1 \leq k \leq m_\tau$.

      3.   Define the restricted edge operators $\mathsf{E}_{\Omega_\tau} : C^{N \times N} \to C^{m_\tau}$ and $\hat{\mathsf{E}}_{\Omega_\tau} : C^{N \times N} \to C^{m_\tau}$ where

$$\begin{aligned} (\mathsf{E}_{\Omega_\tau}X)_k &= (\mathsf{E}X)_{i_k, j_k} \\ (\hat{\mathsf{E}}_{\Omega_\tau}\hat{Y})_k &= (\hat{\mathsf{E}}\hat{Y})_{i_k, j_k} \end{aligned}.$$

5   The Main Algorithm: Combining Fourier and Edge Data

We are ready introduce our algorithm for the reconstruction of X from $m = n$

---

[4]The edge detection matrix applies to one-dimensional Fourier transform information, but we are given two-dimensional Fourier transform information $\hat{Y}$.

Fourier measurements, $\mathsf{F}_\Omega X$, and edge information $\hat{\mathsf{E}}\hat{Y}$. Denote the m Fourier measurements by $y = \mathsf{F}_\Omega X$, and the m_τ edge measurements $y_e = \hat{\mathsf{E}}_{\Omega_\tau}\hat{Y}$. The problem can now be stated in more precise terms: Consider a set Ω of $m = n$ Fourier measurements y of an image X, and a set Ω_τ of m_τ edge measurements, y_e. Assume that the reference image exhibits similar edge information as X. Can we recover X from far fewer Fourier measurements than CS techniques alone would allow by using prior edge measurements y_e?

The answer is yes and the proposed method is to solve the ℓ_1-regularization problem

$$X^*_{\lambda,\gamma} = \arg \min_{Z \in C^{N \times N}} \quad \lambda \mathsf{P} TV_{aniso}(Z)\mathsf{P}_1 + \mathsf{PF}_\Omega X - y\mathsf{P}_2^2 \\ + \gamma \mathsf{PE}_{\Omega_\tau} X - y_e\mathsf{P}_2^2 \quad , \tag{12}$$

where a square error term, $\gamma \mathsf{PE}_{\Omega_\tau} X - y_e\mathsf{P}_2^2$, has been added to include the edge information. Here, λ and γ represent positive scalars which balance regularization and the edge data fidelity. If $\gamma = 0$, our problem is equivalent to (4), and if $\lambda = \gamma = 0$, then $X^*_{0,0}$ is the least squares solution. The success of the algorithm is its ability to find the middle ground between the Fourier information y and the edge information y_e. At the cost of a slightly higher sparsity than the isotropic total-variation discretization, we have found that (??) tends to converge more quickly and accurately to the desired solution. In order to solve ( ), we use a non-linear conjugate gradient method, similar to [13, Section 4.5.2,] but with gradient restarts [15, Section 5.2]. Because the ℓ_1-norm is non-differentiable at zero, we introduce a smoothing parameter μ, and approximate (1) with

$$\mathsf{P} X\mathsf{P}_1 \quad \approx \quad \sum_{i=1}^{N}\sum_{j=1}^{N}\sqrt{X_{i,j} + \mu} \quad .$$

The choice of μ can vary, but in practice we have found that $\mu \in [10^{-12}, 10^{-10}]$ works fairly well. For the choice of parameters λ and γ, we have found that $\lambda \approx \gamma \approx 10^{-2}$ works very well. This condition was determined experimentally, but we also propose a cross-validation type approach to determine λ, γ, similar to [4] (see Appendix 8 for more details).

5.1   Modified Algorithm

Suppose $\hat{Y} \in C^{N_2 \times N_2}$ and $N_2 > N$, i.e. our reference image is of higher resolution than our image X. How does one apply the edge information $\hat{\mathsf{E}}\hat{Y} \in C^{2N_2 \times N_2}$ to our lower resolution image? One solution is to perform a bilinear interpolation on $\hat{\mathsf{E}}\hat{Y} \in C^{2N_2 \times N_2}$ (see Appendix 9 for a more detailed explanation). After the interpolation, we will have lower resolution edge measurements $\mathsf{I}_N(\mathsf{E}_H\hat{Y}) \in C^{2N \times N}$, corresponding to our lower resolution time series images. Then, y_e can be determined by replacing $\mathsf{E}\hat{Y}$ with $\mathsf{I}_N(\mathsf{E}_H\hat{Y})$ in Step 2 of the edge operator algorithm (see the end of Section 4).

A consequence of using higher resolution Fourier edge data for lower resolution images

is that the location of the edges determined by the reference image may no longer be exact anymore. Unfortunately, the algorithm, as is, does not perform well under the interpolated edge information. However, by slightly modifying our algorithm we can achieve extremely accurate reconstruction. The modification is based on the EdgeCS (Edge Guided Compressed Sensing) reconstruction algorithm [9]. In EdgeCS, the idea is to introduce iteratively adapted weights to the total variation ℓ_1 term in (12). These weights are iteratively determined by detecting the jumps of the recovered image (see [9] for more details). In short, wherever the significant jumps are detected, the weights are set to zero to allow the algorithm to fill in the appropriate non-zero value. The new algorithm for interpolated edge measurements is as follows:

1. Set the iteration number $k=1$, the weights $w_i=1$ for $i=1,\dots,n$, and let $X^{(0)}$ be the initial guess.

2. Solve the weighted TV minimization problem with weights w_i and initial guess $X^{(0)}$:

$$X^{(k)}(w) = \arg\min_{Z} \quad \sum_{i=1}^{n} w_i \left(|(D_h Z)_i| + |(D_v Z)_i| \right)$$
$$+ \| PF_\Omega X - y \|_2^2 + \gamma \| PE_{\Omega_\tau} X - y_e \|_2^2$$

3. Detect the jumps of the reconstructed image $X^{(k)}(w)$

$$I^{(k)} \quad \mathrm{¡} \quad \{ i : |(D_h Z)_i| + |(D_v Z)_i| > 2^{-k} \max\{ |(D_h Z)_i| + |(D_v Z)_i| \} \} i = 1,\dots,N \}$$

where $I^{(k)}$ is the index set of the detected jumps.

4. Update the weights: $w_i = 0$ for all $i \in I^{(k)}$ and $w_j = 1$ for all $j \notin I^{(k)}$.

5. Set $X^{(0)} = X^{(k)}$, $k = k+1$ and $\gamma = 0$ and repeat Steps 2 through 5, until the stopping conditions are met.

For $k=1$, the algorithm is equivalent to (12). For $k>1$, the modified algorithm does not use the edge information anymore, i.e., $\gamma = 0$, but, instead, uses edge information from the reconstructed image itself, i.e., Step 3. Numerical examples showed convergence with only four to six iterations in the modified algorithm.

6   Numerical Examples

In this section we present three sets of numerical experiments. The first set illustrates the reconstruction of a time series from incomplete Fourier measurements and edge information using (12). Uniform, Gaussian, and radial sampling patterns are used, and the reference image provides us with exact edge locations for the times series. The next set of experiments show reconstruction of the same time series, but with inexact edge measurements and a Gaussian sampling pattern for the Fourier measurements, using the modified algorithm.

Noise is also introduced in to the measurements. Finally, the third set of experiments examines the reconstruction for a different time series under a Gaussian sampling pattern, inexact edge information, and noisy measurements. In this particular time series, very small changes are occurring between time points, which more accurately simulates an actual fMRI study. The inexact edge information examples correspond to the case in which the reference image dataset is acquired at higher spatial resolution than the time series dataset.

6.1 Reconstruction with exact edge data

6.1.1 Setup

The first set of experiments examines the reconstruction of time series images $\{X(t)\}_{t=1}^{4}$, $X(t) \in C^{64 \times 64}$, from incomplete Fourier measurements and prior edge information from the Fourier transform information $\hat{Y} \in C^{64 \times 64}$ of a reference image $Y \in C^{64 \times 64}$. The reference image contains the same edge or jump locations as the time series. The time series images are Shepp-Logan phantom images with ellipse intensities varying by 1%. Figure 5 shows the reference image and Figure 6 shows the time series images we are trying to reconstruct.

Figure 6: Reference image $Y \in C^{64 \times 64}$. We are given the two-dimensional Fourier transform information of this image, $\hat{Y}$.

Figure 7: $\{X(t)\}_{t=1}^{4}$, $X(t) \in C^{64 \times 64}$, $t = 1,\ldots,4$ from left to right with varying ellipse intensities.

The reference image, Y, and $X(t)$ are the same except for the ellipse intensities of the two center ellipses, $e_l(t), e_r(t) \in R$. The table below compares the values of the two center ellipses between the reference image Y, and the times series images $X(t)$.

	$e_l(t)$	$e_r(t)$
X_1	9.0	10.0
X_2	9.1	9.9
X_3	9.2	9.8
X_4	9.3	9.7
Y	12	12

In these examples, the magnitude of the jumps in the reference image are within 20% to 30% of the exact images $X(t)$. Figure 7 shows a cross sectional view of the reference image versus the image at the first time point, $X(1)$. Both have similar edge information, i.e. the same location of edges, but different jump magnitudes.
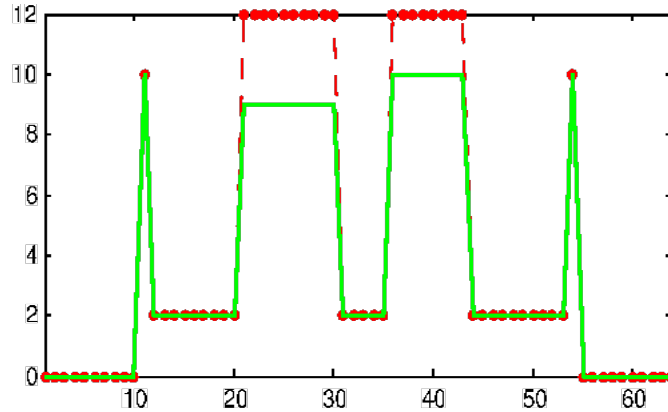
Figure 8: Cross sectional view of the two center ellipses of the reference image Y (shown in red) vs $X(1)$, shown in blue.

The goal of the algorithm will be to reconstruction $X(t)$ from a small number of Fourier measurements and edge information from $\hat{Y}$. Reconstruction of $\{X(t)\}_{t=1}^{4}$ using (12) is presented below under different sampling patterns for the Fourier measurements, i.e. different choices of Ω. Results indicate that a sampling pattern that places a higher number of samples near the zero frequency work extremely well.[5] In all the examples, we take $\lambda = \gamma = .01$, $\tau = .1$ and solve (12).

6.1.2 Uniform Sampling

---

[5]This is not surprising since most of the signals energy, i.e. in the ℓ_2 sense, is contained in the lower spatial frequencies.

Let us take m uniformly sampled Fourier measurements from the time series images $\{X(t)\}_{t=1}^{4}$ shown in Figure 6. Figure 8 shows the sampling pattern with $m = 410$, or roughly 10% of the Fourier coefficients of the image.   In an actual MRI acquisition such sampling can be approximated using a non-Cartesian Fourier space -trajectory.

Figure   9: Fourier domain sampling pattern with uniformly sampling

By utilizing the edge information, we can obtain near exact reconstruction. Figure 9 compares the reconstruction with and without the edge data for all images in the times series $\{X(t)\}_{t=1}^{4}$, for $t = 1,...,4$ viewed along the center cross-section with the 10% uniformly sampled Fourier coefficients and edge data, using $\lambda = \gamma = .01, \tau = .1$. Figure 10 shows a close up of the reconstruction in Figure 9 (left) where the ellipse intensities are changing, and Figure 11 shows the same reconstruction shown in Figure 9 (left), but on individual plots.
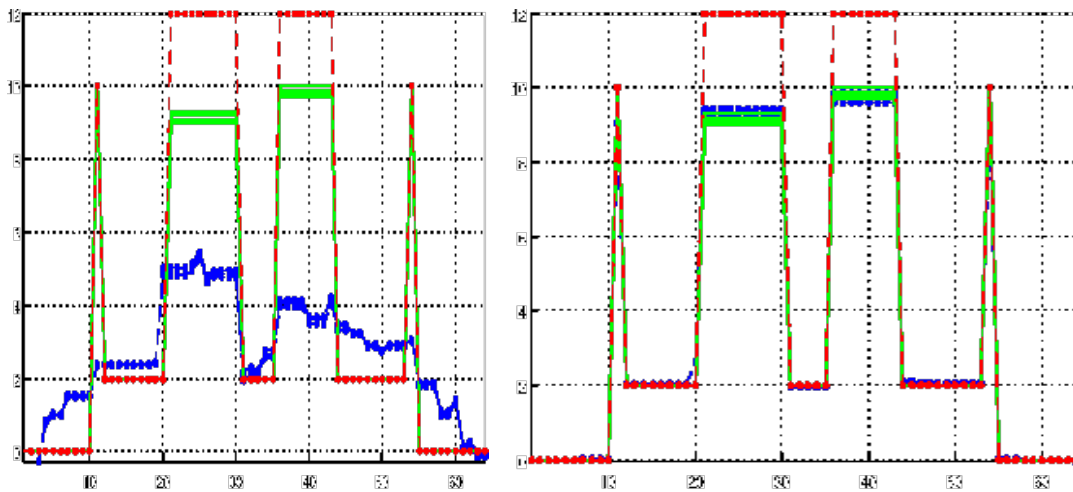
Figure   10: (Left) Reconstruction along the center cross-section with the same 10% uniformly sampled Fourier coefficients and no edge data, i.e. $\gamma = 0$. (Right) Reconstruction of the times series $\{X(t)\}_{t=1}^{4}$ viewed along the center cross-section with the 10% uniformly sampled Fourier coefficients and edge data, with $\lambda = \gamma = .01, \tau = .1$. The blue dotted line represents the reconstruction of the time series, the green line represents the true values, $\{X(t)\}_{t=1}^{4}$, and the red line represents the values for the reference image Y.
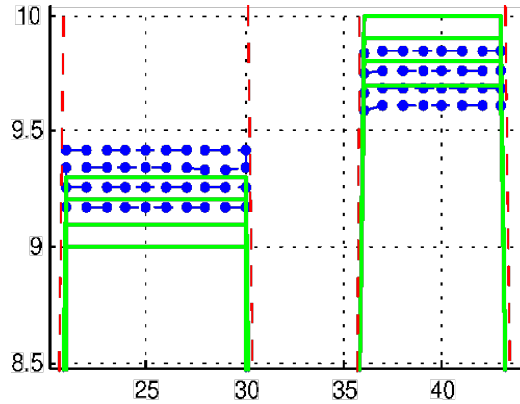
Figure 11: Close up of the left illustration in Figure 9 (left) at the location of the changing ellipse intensities.
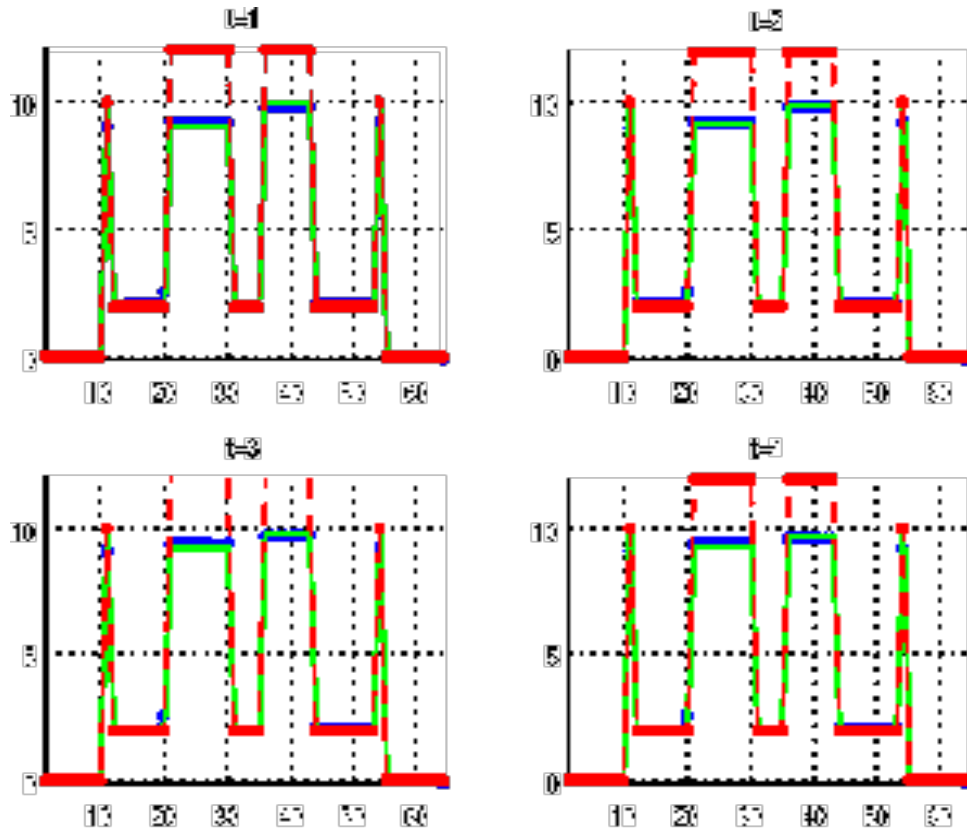

Figure 12: Figure 9 (left) on separate plots for $t = 1, \ldots, 4$.

Experiments indicate that one would require roughly 30% uniformly sampled Fourier measurements to obtain near exact reconstruction using total-variation techniques alone, without any edge data. This means that an overall reduction by a factor of 3.3, compared with full Fourier measurement acquisition, can be achieved using total-variation techniques without

edge data. In comparison, using our approach, one can achieve an overall reduction by a factor of 10, compared with full Fourier measurement acquisition. The additional factor of 3 reduction comes from using the edge information. Thus, if the goal of an fMRI experiment is to find sites of activation where exact knowledge of the ``ideal'' intensity change is of secondary importance, then reductions well below 30% are feasible. If the goal of an fMRI experiment is to find sites of activation where exact knowledge of the "ideal" intensity change is of secondary importance, then reductions below 30% sampling are feasible.

Let $X_1^*(t)$ be the solution to (12) using the 10% uniformly sampled Fourier measurements and edge information, $X_2^*(t)$ be the solution to (12) using the same 10% Fourier measurements and no edge data, and $X_3^*(t)$ be the solution to (12) using 30% uniformly sampled Fourier measurements and no edge data. Table 0 shows the relative errors between the exact solution and the time series reconstructions $X_i^*(t)$, $i = 1,2$ and 3.

t	$RelErr(X_1^*(t))$	$RelErr(X_2^*(t))$	$RelErr(X_2^*(t))$
1	2.38%	53.47%	0.17%
2	2.24%	53.54%	0.16%
3	2.11%	52.34%	0.16%
4	1.99%	53.38%	0.16%

Table 1: Comparison of relative errors between the exact time series and the recovered images. The relative error is defined as $RelErr(X) := \mathsf{P}X^{exact}(t) - X\mathsf{P}_2/\mathsf{P}X_{exact}(t)\mathsf{P}$, where $X_{exact}(t)$ is the exact solution at time t.

6.1.3 Gaussian Sampling

Next, let us show reconstruction results with m Gaussian sampled Fourier coefficients taken from the sequence of images $\{X(t)\}_{t=1}^4$ shown in Figure 6. Figure 12 shows the sampling pattern with $m = 320$, or roughly 8% of the Fourier coefficients of the image.
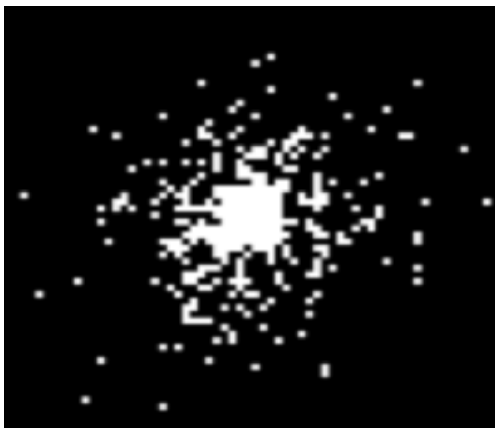
Figure   13: Fourier domain sampling pattern with Gaussian sampling

Figure 13 compares the reconstruction with and without the edge data. Figure 14 shows a close up of the reconstruction in Figure 13 (right),   where the ellipse intensities are changing, and Figure 15 shows the same reconstruction shown in Figure 13 (right), but on individual plots.
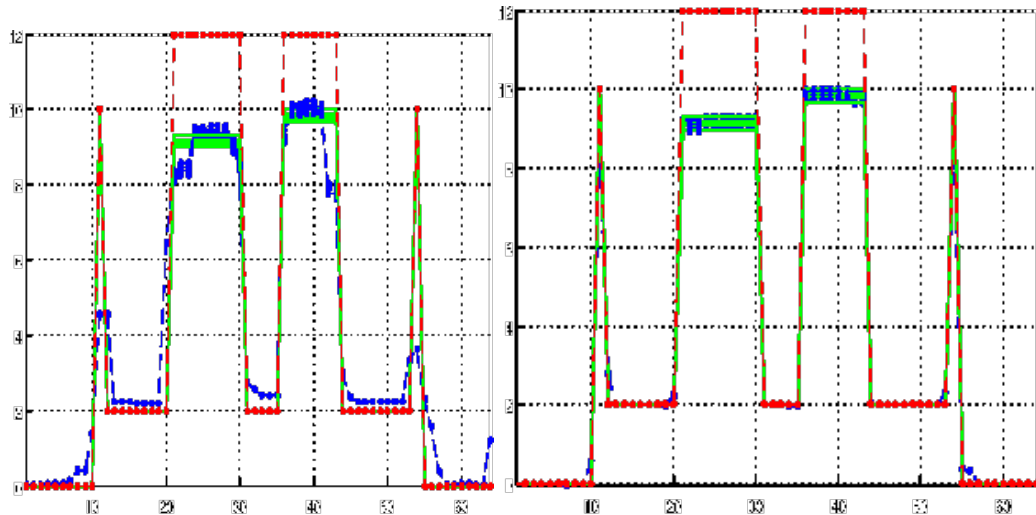

Figure   14: (Left) Reconstruction along the center cross-section with 8% Gaussian sampled Fourier coefficients and no edge data, i.e. $\gamma = 0$. (Right) Reconstruction viewed along the center cross-section with 8% Gaussian sampled Fourier coefficients and edge data, i.e. $\lambda = \gamma = .01, \tau = .1$. The blue dotted line represents the reconstruction, the green line represents the true values, $\{X(t)\}_{t=1}^{4}$, and the red line represents the values for the reference image Y.
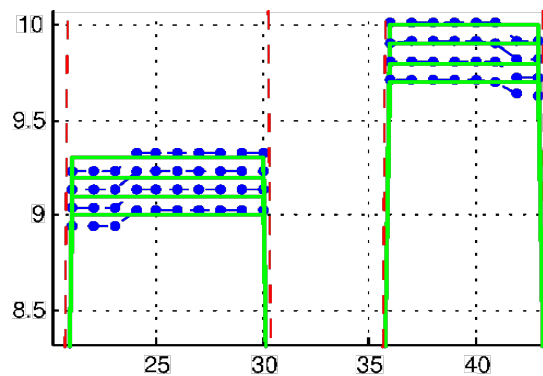
Figure   15: Close up of the left illustration in Figure 13 (left) at the location of the changing ellipse intensities.
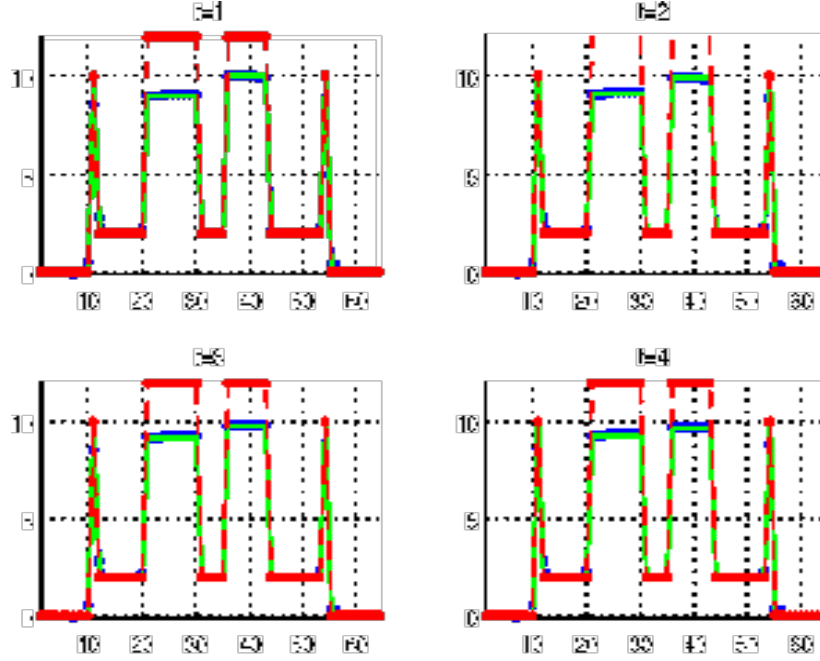
Figure   16: Figure 13 (left) on separate plots for $t=1,\ldots,4$.

Experiments indicate that one would require roughly 20% Gaussian sampled Fourier measurements, using the same density, to obtain near exact reconstruction using total-variation techniques alone, without any edge data. This means that an overall reduction by a factor of 5, compared with full Fourier measurement acquisition, can be achieved using total-variation techniques without edge data. In comparison, using our approach, one can achieve an overall reduction by a factor of 12.5, compared with full Fourier measurement acquisition. The additional factor of 2.5 reduction comes from using the edge information.

Let $X_1^*(t)$ be the solution to (12) using the 8% Gaussian sampled Fourier measurements and edge information, $X_2^*(t)$ be the solution to (12) using the same 8% Fourier measurements and no edge data, and $X_3^*(t)$ be the solution to (12) using 20% Gaussian sampled Fourier measurements and no edge data. Table 1 shows the relative errors between the exact solution and the time series reconstructions $X_i^*(t)$, for $i=1,2$ and 3.

t	$RelErr(X_1^*(t))$	$RelErr(X_2^*(t))$	$RelErr(X_2^*(t))$
1	0.72%	31.29%	0.14%
2	0.71%	31.16%	0.14%
3	0.70%	31.25%	0.15%
4	0.69%	31.26%	0.14%

Table   2: Comparison of relative errors between the exact time series and the recovered images. The relative error is defined as $RelErr(X):=\|X^{exact}(t)-X\|_2/\|X_{exact}(t)\|$,

where $X_{exact}(t)$ is the exact solution at time t.

6.1.4   Radial Sampling

Finally, we show reconstruction results with m radially sampled Fourier coefficients taken from the sequence of images $\{X(t)\}_{t=1}^{4}$ shown in Figure 6. Figure 16 shows the sampling pattern 5 radial lines with $m = 336$, or roughly 8% of the Fourier coefficients of the image.
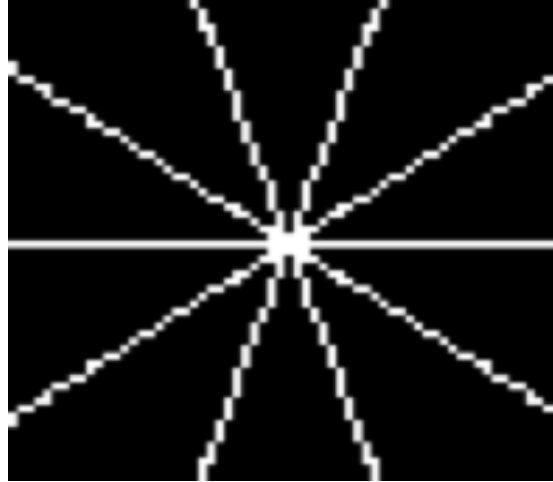

Figure   17: Fourier domain sampling pattern with radial sampling.

Figure 17 compares the reconstruction with and without the edge data. Figure 18 shows a close up of the reconstruction in Figure 17 (right),   where the ellipse intensities are changing, and Figure 19 shows the same reconstruction shown in Figure 17 (right), but on individual plots.
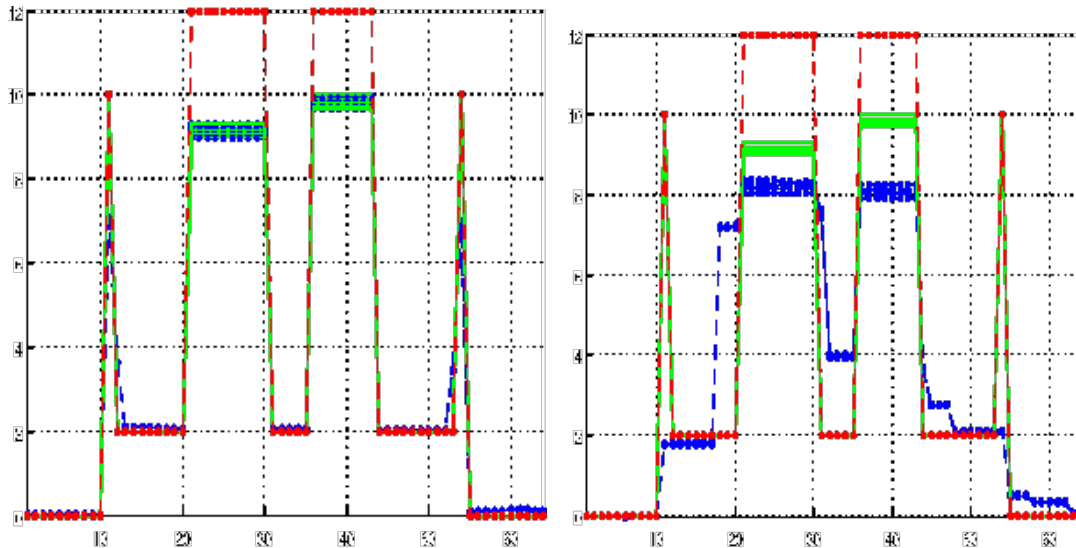

Figure   18: (Left) Reconstruction viewed along the center cross-section with 8% radial sampled Fourier coefficients and edge data, i.e. $\lambda = \gamma = .01, \tau = .1$. (Right) Reconstruction

along the center cross-section with 8% radial sampled Fourier coefficients and no edge data, i.e. $\gamma = 0$. The blue dotted line represents the reconstruction, the green line represents the true values, $\{X(t)\}_{t=1}^{4}$, and the red line represents the values for the reference image Y.
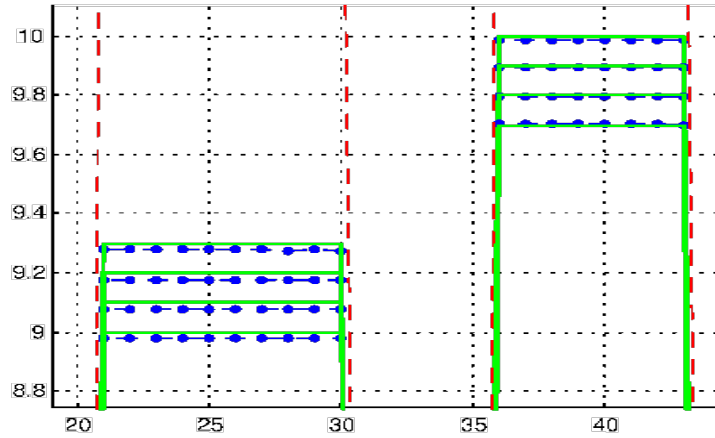

Figure 19: Close up of the left illustration in Figure 17 (left) at the location of the changing ellipse intensities.
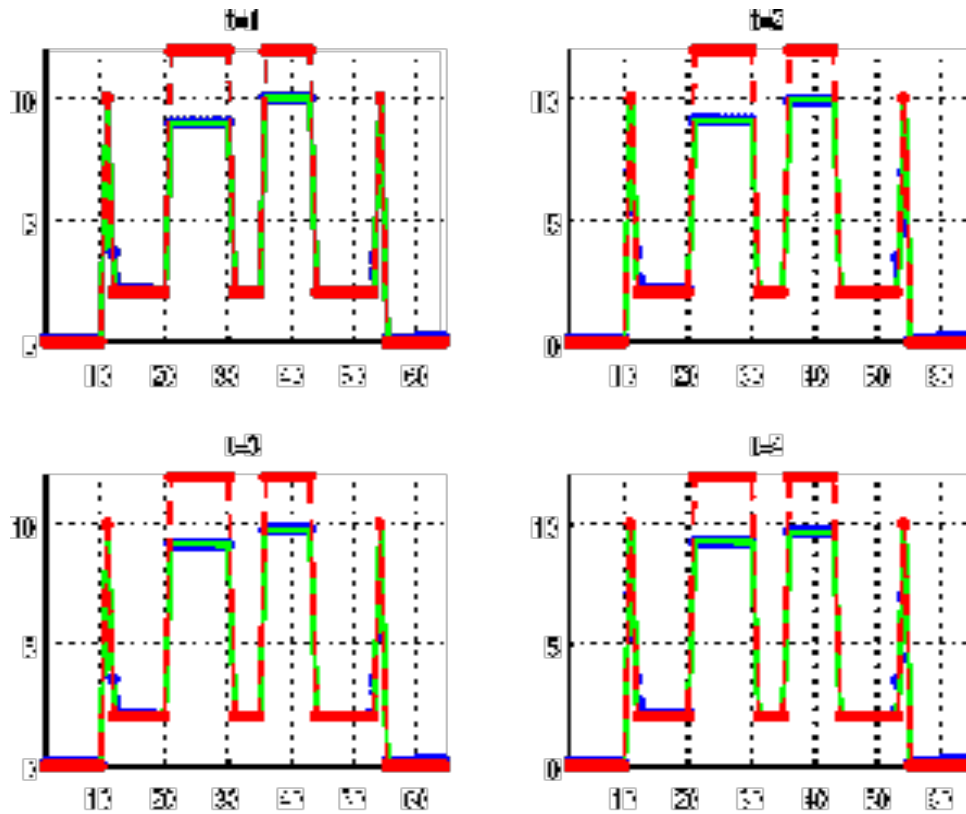

Figure 20: Figure 17 (left) on separate plots for $t = 1, \ldots, 4$.

Experiments indicate that one would require roughly 15 radial lines or roughly 23% Fourier measurements to obtain near exact reconstruction using total-variation techniques alone, without any edge data. This means that an overall reduction by a factor of about 4.3, compared with full Fourier measurement acquisition, can be achieved using total-variation techniques without edge data. In comparison, using our approach, one can achieve an overall reduction by a factor of 12.5, compared with full Fourier measurement acquisition. The additional factor of 3 reduction comes from using the edge information.

Let $X_1^*(t)$ be the solution to (12) using the 8% radially sampled Fourier measurements and edge information, $X_2^*(t)$ be the solution to (12) using the same 8% Fourier measurements and no edge data, and $X_3^*(t)$ be the solution to (12) using 23% radially sampled Fourier measurements and no edge data. Table 2 shows the relative errors between the exact solution and the time series reconstructions $X_i^*(t)$, for $i=1,2$ and 3.

t	$RelErr(X_1^*(t))$	$RelErr(X_2^*(t))$	$RelErr(X_2^*(t))$
1	0.68%	14.10%	0.19%
2	0.71%	14.08%	0.20%
3	0.75%	14.06%	0.20%
4	0.80%	14.04%	0.20%

Table 3: Comparison of relative errors between the exact time series and the recovered images. Relative error is defined as $RelErr(X) := \mathsf{P}X^{exact}(t) - X\mathsf{P}_2 / \mathsf{P}X_{exact}(t)\mathsf{P}$, where $X_{exact}(t)$ is the exact solution at time t.

6.2   Reconstruction with high resolution reference image

Consider the reconstruction of the same time series $\{X(t)\}_{t=1}^4$ as the the first set of tests, but with Fourier transform information $\hat{Y} \in C^{256 \times 256}$ from a high resolution reference image $\hat{Y} \in C^{256 \times 256}$. In order to use the edge information from $\hat{Y}$ for our algorithm, we perform a bilinear interpolation on $\hat{\mathsf{E}}\hat{Y}$. As stated in Section 5.1, this introduces inexact edge information. Figure 20 shows the reference image that corresponds to edge information of the interpolant versus the true edge information of the time series images, along a cross-section. The location of the edges for the two center ellipses are not exact anymore. We use the modified algorithm for reconstruction of the time series.
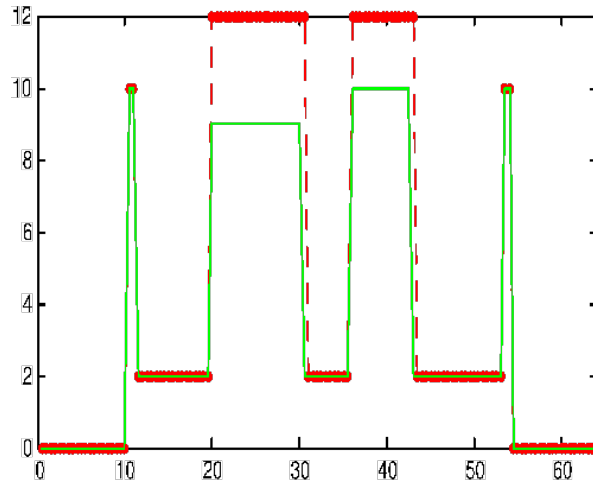
Figure 21: Red shows edge information of the reference image, determined by the interpolations on the edge data, i.e. the interpolant $I_N(E_H\hat{Y})$, and the green shows the exact edge information for the time series images. The edges are not aligned anymore as in Figure 7.

Figure 21 shows the Gaussian sampling pattern with $m = 484$, or roughly 12% of the Fourier coefficients of the image.
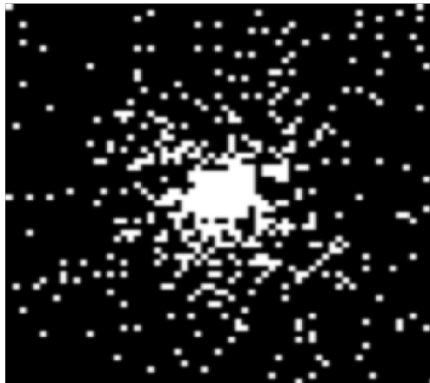

Figure 22: Fourier domain sampling pattern with Gaussian sampling

Figure 22 shows the reconstruction under the 12% Gaussian sampling pattern with the modified algorithm which performs an iterative re-weighting of the total variation ℓ_1 term.
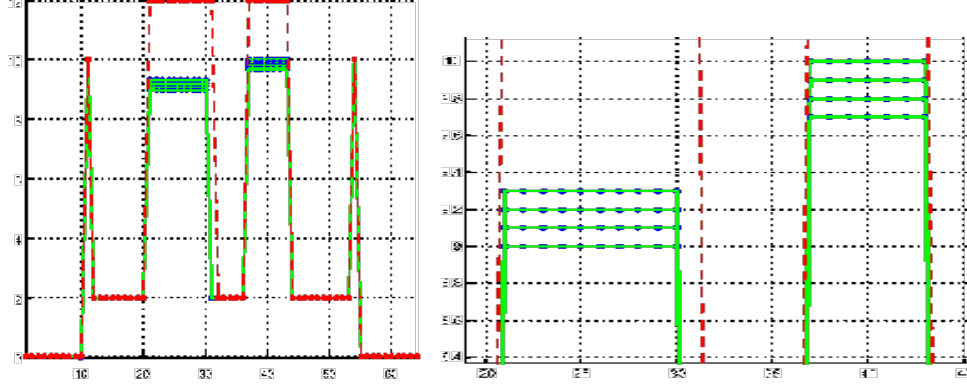
Figure 23: (Left) Reconstruction of the time series $X(t)$ viewed along the center cross-section with 12% Gaussian sampled Fourier coefficients and edge data, i.e. $\lambda = \gamma = .01, \tau = .1$, using the modified algorithm. (Right) Close up of the center ellipses.

Let $X_1^*(t)$ be the solution to the modified algorithm using the 12% Gaussian sampled Fourier measurements and edge information. Table 3 shows the relative errors between the exact time series solution and the recovered image.

t	$RelErr(X^*(t))$
1	$5.21e-5\%$
2	$1.00e-4\%$
3	$7.82e-5\%$
4	$7.82e-4\%$

Table 4: Relative errors between the exact time series and the recovered images using the modified algorithm with 12% Gaussian sampling pattern and edge information. Relative error is defined as $RelErr(X) := \Vert X^{exact}(t) - X \Vert_2 / \Vert X_{exact}(t) \Vert$, where $X_{exact}(t)$ is the exact solution at time t.

Again, experiments indicate that one would require roughly 20% Gaussian sampled Fourier measurements to obtain near exact reconstruction using total-variation techniques alone, without any edge data. This means that an overall reduction by a factor of 5, compared with full Fourier measurement acquisition, can be achieved using total-variation techniques without edge data. In comparison, using our approach, one can achieve an overall reduction by a factor of 8, compared with full Fourier measurement acquisition. The additional factor of 1.6 reduction comes from using the edge information.

Remark 1 *Inexact edge measurements may also be attributed to the motion of a test subject in an fMRI study. Thus, these results indicate that one may still be able to use edge information in the presence of motion inaccuracies for exact reconstruction under the modified algorithm.*

6.2.1 With Noise

In this section we show reconstruction of the same time series as in the previous section, but in the presence of measurement noise. In this example, Gaussian white noise is simply added to the measurements y. The signal-to-noise (SNR) is defined as the ratio between the maximum zero frequency of $X(t)$ divided by the standard deviation of the Gaussian white noise. Figure 23 shows reconstruction with the 12% Gaussian Fourier sampling pattern for an SNR of 150 and 100.
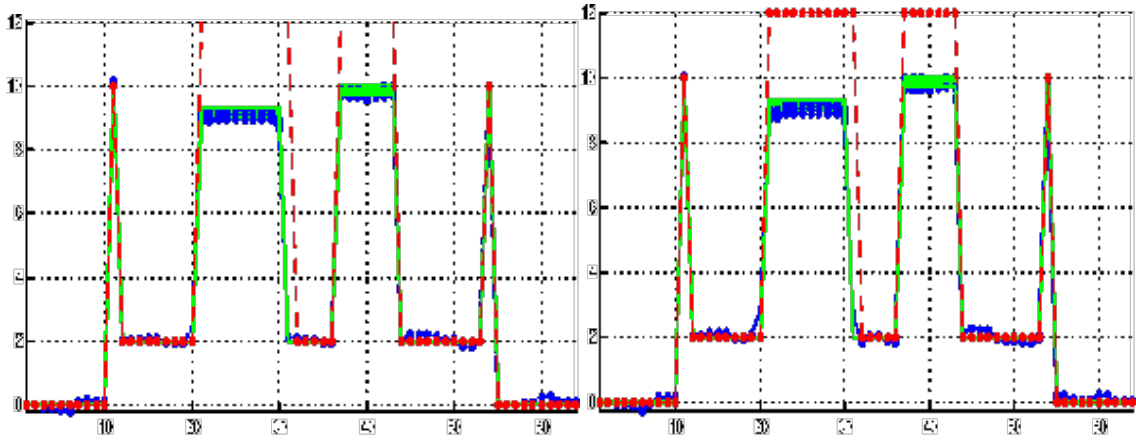

Figure 24: Reconstruction with noise. $SNR=150$ on the left, and $SNR=100$ on the right

Let $X_1^*(t)$ be the solution to the modified algorithm with SNR of 150 and $X_2^*(t)$ be the solution to the modified algorithm with an SNR of 100. The table below displays the relative errors between the exact time series solution and the recovered time series.

t	$RelErr1(snr=150)$	$RelErr(snr=100)$
1	3.90%	5.51%
2	3.88%	5.63%
3	3.85%	5.65%
4	3.86%	5.76%

Table 5: Relative errors between the exact time series and the recovered images using the modified algorithm with 12% Gaussian sampling pattern and edge information with an SNR of 150 and 100. Relative error is defined as $RelErr(X):=\|X^{exact}(t)-X\|_2/\|X_{exact}(t)\|$, where $X_{exact}(t)$ is the exact solution at time t.

6.3   Example with iso-intense ellipse intensities

6.3.1   Noiseless Case

In this last example, let us consider a time series in which a smaller ellipse is iso-intense with its surroundings: (1) the ellipse is the same intensity as its surrounding at some point and (2) the ellipse changes intensity by 1% at another time point. This increase in intensity corresponds to the activation of the region in response to some stimulus in a fMRI time series study.   In the noiseless case, the time series will consist of two Shepp-Logan phantom images, where only the intensity of the center most ellipse is changing. Figure 24 displays the two images in the time series along with their center cross-sections.
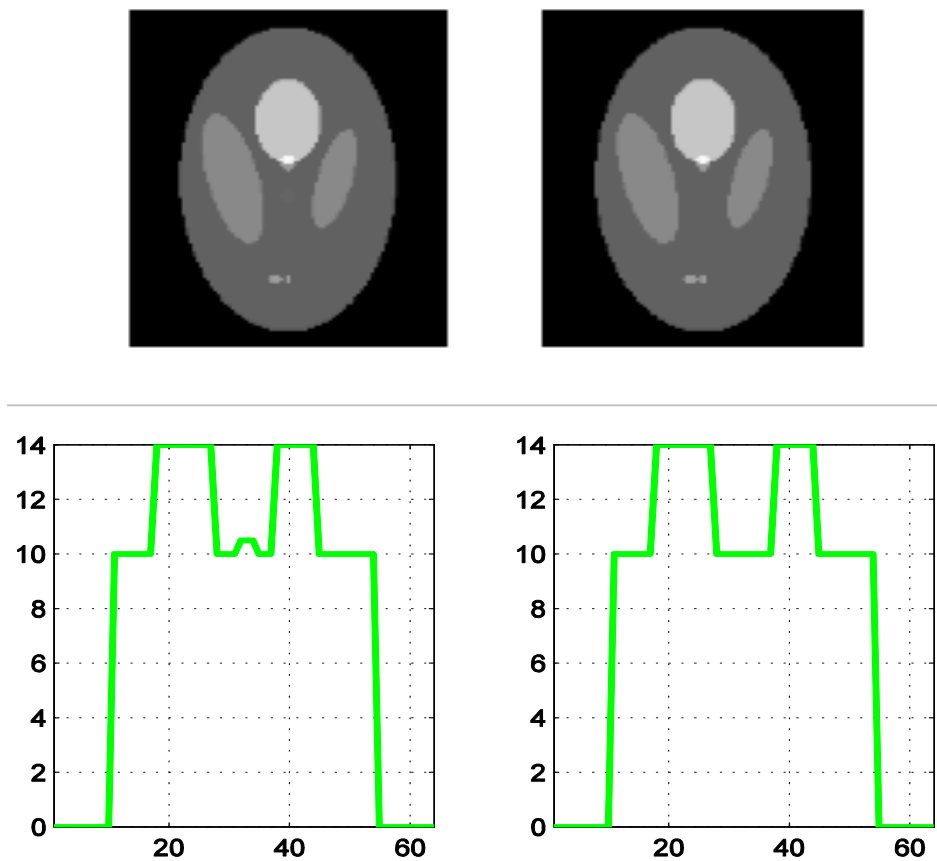

Figure   25: Images in our time series (top) and center cross-section of those images (bottom) to illustrate the center ellipse intensities. The ellipse that is iso-intense with its surrounding is displayed in the center.

A high resolution reference image also provides us with approximate edge information.[6] The center ellipse intensities for the two images in the time series differ by 1%, while the high resolution reference image intensity remains static. Denote the center ellipse intensity by $e_c(t)$. The ellipse intensities are displayed in the table below.

$X(t)$	$e_c(t)$
$X(1)$	10.0
$X(2)$	10.1
Y	12

Table 6: Ellipse intensities for the time series and reference image.

Using the same 12% Gaussian sampling pattern for the Fourier measurements as in Figure 21 and inexact edge measurement the reconstruction with the modified algorithm is shown in the figure below.
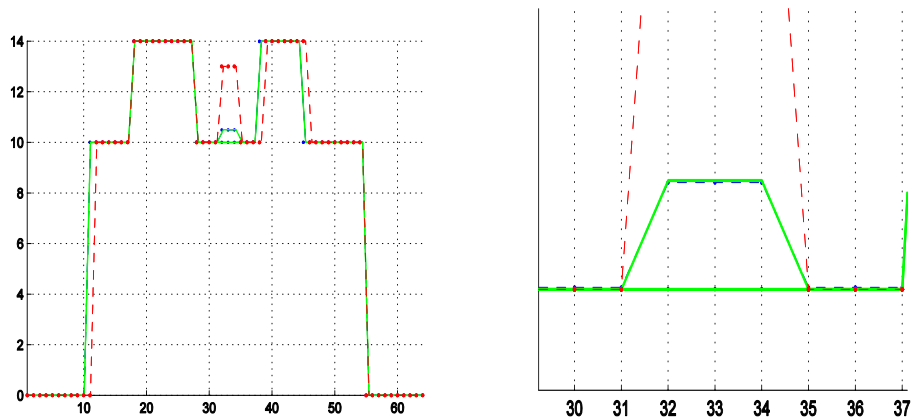

Figure 26: (Left) Reconstruction of the time series $X(t)$ viewed along the center cross-section with 12% Gaussian sampled Fourier coefficients and edge data, i.e. $\lambda = \gamma = .01, \tau = .1$, using the modified algorithm. (Right) Close up of the center ellipse. Red indicates the edge information, green indicates the exact solution, and blue indicates the recovered image.

We also illustrate the reconstruction with and without edge information with the same 12% Gaussian sampling pattern.

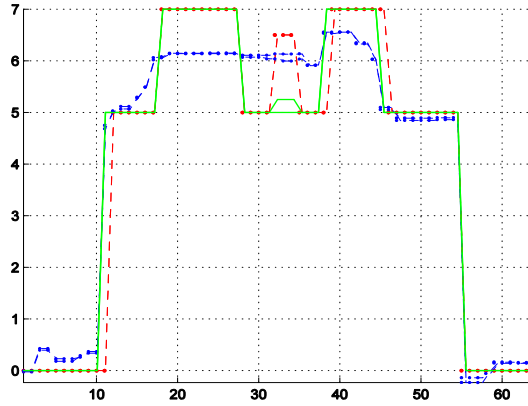[6]Approximate and not exact because of interpolation errors.

Figure   27: Reconstruction with edge data (right) and without edge data (left) using a 12% Gaussian sampling pattern.

Experiments indicate that one would require roughly 20% Gaussian sampled Fourier measurements to obtain near exact reconstruction using total-variation techniques alone, without any edge data. This means that an overall reduction by a factor of 5 can be achieved using total-variation techniques without edge data. In comparison, using our approach, one can achieve an overall reduction by a factor of 8, compared with full Fourier measurement acquisition. The additional factor of 1.6 reduction comes from using the inexact edge information.

Let $X_1^*(t)$ and $X_2^*(t)$ be the solution to the modified algorithm for the iso-intense time series example with and without edge data. The table below displays the relative errors between $X_i^*(t)$, $i = 1,2$, and the exact solution.

t	$RelErr(X_1^*(t))$	$RelErr(X_2^*(t))$
1	$4.92\mathrm{e}-4\%$	16.10%
2	$1.35\mathrm{e}-4\%$	16.29%

Table   7: Relative errors for the iso-intense time series example. Relative error is defined as $RelErr(X) := \mathsf{P}X^{exact}(t) - X\mathsf{P}_2 / \mathsf{P}X_{exact}(t)\mathsf{P}$, where $X_{exact}(t)$ is the exact solution at time t.

6.3.2   With Noise

Now consider a 32 point iso-intense time series example in which the small center ellipse is only varying by 1% again. Figure 27 illustrates the intensities of the center ellipse as a function of time.
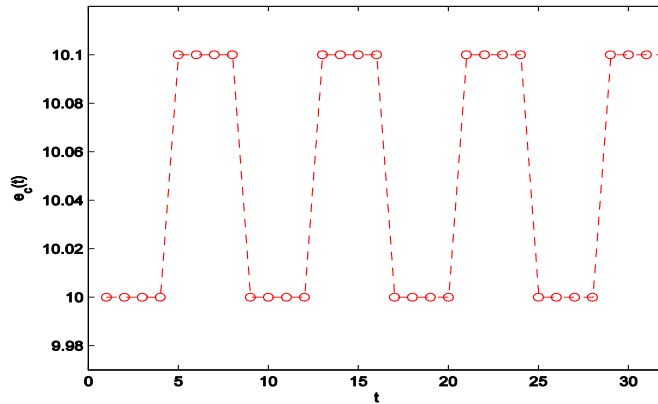
Figure 28: Center ellipse intensity as a function of $t = 1, \ldots, 32$.

Using the modified algorithm with 12% Gaussian sampled Fourier measurements and the high resolution reference image with inexact edge information, Figure 28 illustrates the ellipse intensities for the reconstruction with SNR values at 150 and 100.[7] The value of the ellipse intensity at each time point is the mean ellipse intensity, i.e., the mean value of points in the center ellipse.
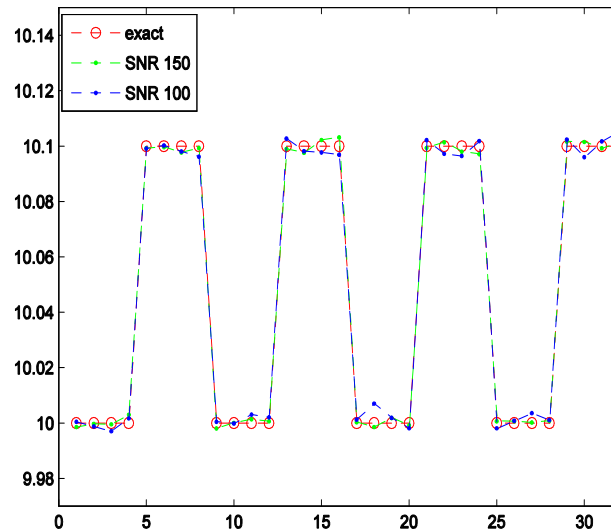

Figure 29: Mean ellipse intensities for the reconstruction with SNR 150 (green) and 100 (blue) versus the true ellipse intensities.

The Pearson correlation coefficient for the reconstructed ellipse intensity time series plot in Figure 28 is .9998 and .9968 for the SNR 150 and 100, respectively.

7   Summary and Conclusion

---

[7]The noise is added to each of the images in the 32 point time series.

In this paper we introduce a new algorithm to reconstruct sparse gradient time series images from limited Fourier measurements and prior edge information from a reference image. Results show that the number of Fourier measurements required to obtain accurate reconstruction can be reduced by a factor of 1.6 - 3 by the addition of Fourier edge information. In particular, numerical experiments indicate that Fourier sampling patterns which place more points near the zero frequencies, e.g., Gaussian or radial patterns, show the most significant reduction in the requisite Fourier measurements for exact and stable recovery. Moreover, the proposed algorithm is robust in the sense that the regularization parameters do not need to be extensively re-tuned for every image in the time series, the edge information can be inexact, and the jump intensities of the reference image can be within 20-30% of the true intensities in the time series images.

Another feature of our algorithm is that it can be easily adapted to existing compressed sensing methods by simply adding a second order conic constraint term which incorporates the priori edge measurements from the reference image. Thus, there is potential to combine the ideas in this paper with more state-of-the-art algorithms (see, for example, [17] or [21]). In particular, there has been recent work in combining compressed sensing with parallel imaging techniques for improved accuracy and robustness [11, 12]. While our algorithm could be used in lieu of this approach, it is also easily conceivable to combine our technique with parallel imaging methods such as SENSE or GRAPPA (to be added) to provide for a further reduction in the amount of Fourier space data acquired for an fMRI time series study.

Appendix

8 Cross-Validation

In order to determine the regularization parameters, we outline a cross-validation approach similar to [4]:

1. Divide the m Fourier measurements, y, into m_r reconstruction and m_v validation samples. This will correspond to a new set of indices Ω_r and Ω_v for reconstruction and validation, respectively.

2. Choose multiple pairs of (λ, γ) to solve (??) using only the m_r reconstruction Fourier measurements. Note that in (??), F_Ω and y will be replaced by F_{Ω_r} and y_r.

3. For each solution in Step 2, compute the reconstruction error $\|\mathsf{F}_{\Omega_v} X^*_{\lambda\gamma} - y_v\|_2$ using the validation samples.

4. Choose the pair (λ, γ) for which the error in Step 3 is the smallest.

9 Edge Interpolation

In this section we provide an example that illustrates how one can utilize the high resolution edge information for lower resolution images. First, Consider the high resolution edge operator $\mathsf{E}_H : C^{N_H \times N_H} \to C^{2N_H \times N_H}$, and the low resolution edge operator $\mathsf{E} : C^{N \times N} \to C^{2N \times N}$ where $N_H > N$. To determine the approximate edge measurements for the lower resolution image, we will essentially perform a bilinear interpolation on $\mathsf{E}_H \hat{Y}$. Define the high resolution one-dimensional N_H point grid

$$x_j \quad = \quad \frac{j}{N_H}, \quad j = 1, \ldots, N_H.$$

Similarly, define the lower resolution one-dimensional N point grid as

$$\widetilde{x}_j \quad = \quad \frac{j}{N}, \quad j = 1, \ldots, N.$$

Denote the ith row of $\mathsf{E}_H \hat{Y}$ by $\{f_{i,j}\}_{j=1}^{N}$. If we consider the pairing $\{(x_j, f_{i,j}\}_{j=1}^{N_H}$ as discrete samples of a one-dimensional function $f_i(x)$ at points x_j, we can perform a linear interpolation of $f_i(x)$ at the courser grid points $\{\widetilde{x}_j\}_{j=1}^{N}$. Afterwards, for each fixed column, we perform the analogous linear interpolation on the first N_H rows, and then on the last N_H rows separately (remember that each column of $\mathsf{E}_H \hat{Y}$ is of length $2N_H$). Once this bilinear interpolation is complete, we will have lower resolution edge measurements denoted by $\mathsf{I}_N(\mathsf{E}_H \hat{Y}) \in C^{2N \times N}$.

References

[1] N. Bary. *Treatise on Trigonometric Series* . Macmillan, 1964.

[2] E. Candes and J. Romberg. *l1-Magic: Recovery of Sparse Signals via Convec Programming* .

[3] E. Candes, J. Romberg, and T. Tao. Robust uncertainty principles: exact signal reconstruction from highly incomplete frequency information. *IEEE Transactions on Information Theory* , 52:489--509, 2006.

[4] A. Doostan and H. Owhadi. A non-adapted sparse approximation of pdes with stochastic inputs. *Journal of Computational Physics* , 230(8):3015--3034, 2011.

[5] M. Fornasier and H. Rauhut. Compressive Sensing. In O. Scherzer, editor, *Handbook*

of Mathematical Methods in Imaging , pages 187--228. Springer, 2011.

[6] A. Gelb and E. Tadmor. Detection of edges in spectral data II. nonlinear enhancement. *SIAM Journal on Numerical Analysis* , 38:1389--1408.

[7] A. Gelb and E. Tadmor. Detection of edges in spectral data. *Applied and Computational Harmonic Analysis* , 7:101--135, 1999.

[8] A. Gelb and E. Tadmor. Detection of edges in spectral data III: Refinement of the concentration method. *Journal of Scientific Computing* , 36:1--43, 2008.

[9] W. Guo and W. Yin. Edgecs: Edge guided compressive sensing reconstruction. In *Visual Communications and Image Processing* , 2010.

[10] J. Hesthaven, D. Gottlieb, and S. Gottlieb. *Spectral Methods for Time-Dependent Problems* . Cambridge University Press, 2000.

[11] K. F. King. Combining compressed sensing and parallel imaging. *Proceedings of the International Society on Magnetic Resonance in Medicine* , 16, 2008.

[12] R. Liu, F. M. Sebert, Y. Zou, and L. Ying. Sparsesense: Randomly-sampling parallel imaging using compressed sensing.

[13] M. Lustig, D. Donoho, and J.M. Pauly. Sparse MRI: the application of compressed sensing for rapid MR imaging. *Mangetic Resonance in Medicine* , 58:1182--1195, 2007.

[14] D. Nishimura. *Principles of Magnetic Resonance Imaging* . 2010.

[15] J. Nocedal and S. Wright. *Numerical Optimization* . Springer, 1st edition edition, 1999.

[16] S. Ogawa, D. W. Tank, R. Menon, J. M. Ellerman, S. G. Kim, H. Merkle, and K. Ugurbil. Intrinsic signal changes accompanying sensory stimulation: functional brain mapping with magnetic resonance imaging. *Proceedings of the National Academy of Sciences* ,

89:5951--5955, 1992.

[17] V. Patel, R. Maleh, A. Gilbert, and R. Chellappa. Gradient-based image recovery methods from incomplete fourier measurements. *IEEE Transactions on Image Processing, accepted for publication*, 2011.

[18] H. Rauhut. Monograph on compressed sensing. Unpublished manuscript, Chapter on Homotopy Methods.

[19] H. Rauhut. Random sampling of sparse trigonometric polynomials. *Applied and Computational Harmonic Analysis*, 22:16--42, 2009.

[20] L. A. Shepp and B. F. Logan. The fourier reconstruction of a head section. *IEEE Transactions on Nuclear Science*, 21(3):21--43, 1974.

[21] Y. Wang, J. Yang, W. Yin, and Y. Zhang. A new alternating minimization algorithm for total variation image reconstruction. *SIAM Journal on Imaging Science*, 1(3):348--272, 2008.